COMMUN. MATH. SCI.
Vol. 15, No. 3, pp. 665–692

A DYNAMICAL STATE UNDERLYING THE SECOND ORDER MAXIMUM ENTROPY PRINCIPLE IN NEURONAL NETWORKS*

ZHI-QIN JOHN XU†, GUOQIANG BI‡, DOUGLAS ZHOU§, AND DAVID CAI¶

Abstract. The maximum entropy principle is widely used in diverse fields. We address the issue of why the second order maximum entropy model, by using only firing rates and second order correlations of neurons as constraints, can well capture the observed distribution of neuronal firing patterns in many neuronal networks, thus, conferring its great advantage in that the degree of complexity in the analysis of neuronal activity data reduces drastically from $\mathcal{O}(2^n)$ to $\mathcal{O}(n^2)$, where n is the number of neurons under consideration. We first derive an expression for the effective interactions of the nth order maximum entropy model using all orders of correlations of neurons as constraints and show that there exists a recursive relation among the effective interactions in the model. Then, via a perturbative analysis, we explore a possible dynamical state in which this recursive relation gives rise to the strengths of higher order interactions always smaller than the lower orders. Finally, we invoke this hierarchy of effective interactions to provide a possible mechanism underlying the success of the second order maximum entropy model and to predict whether such a model can successfully capture the observed distribution of neuronal firing patterns.

Keywords. maximum entropy model; high dimensional data; neuronal networks; mechanism

AMS subject classifications. 62B10; 82B05; 92C20

1. Introduction

In neuroscience, there are various population coding theories and experimental results suggesting that information encoded in correlated neuronal population responses is not simply a linear summation of information embedded in individual neurons. However, how to understand collective behaviors of neuronal populations remains a great scientific challenge. With the development of new experimental techniques, many laboratories have been able to perform long duration ($\sim$1h) recordings from hundreds of neurons simultaneously [10]. How to extract information from such high dimensional data from experimental measurement has become an urgent issue.

There is strong evidence that information is encoded within spike trains (the firing pattern) of neurons. To decipher the coded information, it is essential to investigate characteristics of spike patterns [4, 8]. For a fixed sampling time bin, one can use a binary quantity to describe the two states of each neuron, for example, 1 for the neuron to be active (firing) and 0 for being silent (not firing). For a group of n neurons, a binary vector can be used to characterize the state of the firing pattern in each sampling time bin. To understand how neuronal networks encode information, one needs to study the relation between a stimulus and its corresponding neuronal firing pattern. There are 2^n possible states in each sampling time bin for a network of n neurons. Therefore, the

*Received: July 1, 2016; accepted: August 9, 2016. Communicated by Shi Jin.

†School of Mathematical Sciences, MOE-LSC and Institute of Natural Sciences, Shanghai Jiao Tong University, Shanghai, P.R. China and NYUAD Institute, New York University Abu Dhabi, PO Box 129188 Abu Dhabi, United Arab Emirates (xuzhiqin@sjtu.edu.cn).

‡CAS Key Laboratory of Brain Function and Disease, and School of Life Sciences, University of Science and Technology of China, Anhui, P.R. China (gqbi@ustc.edu.cn).

§Corresponding author, School of Mathematical Sciences, MOE-LSC and Institute of Natural Sciences, Shanghai Jiao Tong University, Shanghai, P.R. China (zdz@sjtu.edu.cn).

¶Corresponding author, School of Mathematical Sciences, MOE-LSC and Institute of Natural Sciences, Shanghai Jiao Tong University, Shanghai, P.R. China, and Courant Institute of Mathematical Sciences and Center for Neural Sciences, New York University, New York, NY and NYUAD Institute, New York University Abu Dhabi, PO Box 129188 Abu Dhabi, United Arab Emirates (cai@cims.nyu.edu).

number of all possible states is exponentially growing with the neuron number. This presents a theoretical challenge to study a network of a large number of neurons. Any method that can reduce this exponentially growing complexity would greatly facilitate our understanding of population behaviors of neurons. To tackle this complexity, the Maximum Entropy Principle (MEP) has been applied to the analysis of neuronal data. Using MEP, one can find the desired probability distribution by maximizing the entropy subject to given constraints [17]. The MEP has been widely used in diverse fields, such as in neuroscience [11,23,27,43–46], biological network studies [6,22,31,40,42], imaging science [32], economics [13, 38], linguistics [39], anthropology [15], and atmosphere-ocean science [18]. The second order maximum entropy (MaxEnt) model, using the mean and correlation as constraints, is a special case of the MEP. There are recent works [34, 36] showing that by using the second order MaxEnt model it is possible to predict 90% to 99% of information (See relevant definitions in Section 3.) encoded in all orders of correlations of neuronal network dynamics in many areas of the brain [17] and the reconstructed distribution of the firing pattern using the second order MaxEnt model can well capture the observed distribution of neuronal firing patterns in different brain states, such as spontaneous states [36, 41] or the state under visual drives [34]. The degree of freedom in the second order MaxEnt model is $\mathcal{O}(n^2)$ since the highest order of correlations it takes into account is pairwise correlations. If this model is generally applicable to characterize neuronal network dynamics arising from the brain, it could drastically simplify the mathematical analysis of how neuronal networks encode information. A series of works have been initiated to address various aspects of the second order MaxEnt model, including explorations of fast algorithms [5, 26], inference of spatial-temporal correlations [23, 25, 37, 41, 46], and functional connectivity [3,9,16,30,45,47]. Despite these investigations and applications of MEP, there are critical issues also being raised [12,21,24,27–29,48], such as the second order MaxEnt model no longer sufficient for networks of large sizes (*e.g.*, $\sim$100 neurons [12]), or networks over fine-scales, *i.e.*, local clusters of neurons within $300\,\mu$m [27].

To use the second order MaxEnt model effectively, we need to understand under what conditions the second order MaxEnt model can well capture the observed distribution of neuronal firing patterns. There are studies that have attempted to address this issue. It was argued [29] that the success of MaxEnt models requires that the network size be smaller than a critical size, in which the critical size only depends on firing rates and sampling time bin size. However, there are also studies [35] in which no clear critical value for network size was found in the sense that the neuronal network sizes are larger than the critical size yet the distribution of the firing pattern obtained from the second order MaxEnt model was still in good agreement with the observed distribution of neuronal firing patterns in neurophysiological experiments. In addition, as often observed, the correlation coefficient between the activity of two neurons typically is weak ($\leq 10\%$) [1,7], one may suspect that the weak correlations may be relevant to the success of the MaxEnt approaches. However, there are theoretical analyses using a perturbation theory [1] to show that the success is not simply a consequence of weak correlations, in the sense that even though all pairwise correlations are weak, the entropy of the distribution of the second order MaxEnt model is not captured in leading orders of the perturbation theory with respect to weak correlations. Therefore, it remains important to clarify under what conditions the second order MaxEnt model can well capture the observed distribution of neuronal firing patterns.

In this work, we aim to explore a possible mechanism underlying the validity of the second order MaxEnt model in neuronal network dynamics. In our numerical ex-

periments, we find that weak high order correlations do not guarantee the success of the second order MaxEnt model. To understand what is underlying the success of the second order MaxEnt model in the reconstruction of the distribution of neuronal firing patterns for a network with n neurons, instead of focusing on correlations, we theoretically analyze the effective interactions in the nth order MaxEnt model using all orders of correlations of neurons as constraints. We first develop a method to derive an explicit mathematical form for all the interactions of the nth order MaxEnt model. Then, we show that the high order (above the second order) interactions of the MaxEnt model are much smaller in strength than the lower order ones in dynamical states for which the second order MaxEnt model can well capture the distribution of neuronal firing patterns. To understand under what conditions the high order interactions in the MaxEnt model are weak, we develop a theoretical framework using homogeneously coupled neuronal networks. In our framework, there emerge two important quantities: one is the conditional probability, p, of one neuron from the silent state to the active state conditioned on other neurons being silent, the other is the increment, δ, of conditional probability of the neuron in the active state induced by one of the other active neurons. We discover a linearity condition involving these two quantities p and δ that plays an important role in the network dynamical state underlying the success of the MaxEnt models. Specifically, the linearity condition states that the conditional probability increment of one neuron from the silent state to the active state induced by a group of neurons is equal to the linear summation of increments induced by each of the individual neurons in the group. Under this condition, for an asynchronous network, we develop a perturbation theory to show that the strengths of interactions in the MaxEnt model form a hierarchy in the power of δ, that is, the second order interactions are dominant terms which are of order δ, the third order interactions are of order δ^2 and so forth. We show that this hierarchy of order can be used to predict whether the second order MaxEnt model can characterize well the distribution of neuronal firing patterns. Using Hodgkin–Huxley (HH) network models, we demonstrate numerically that the linearity condition persists as long as the neurons are not firing synchronously.

We also investigate other important issues related to the MaxEnt model. We study whether the sampling time bin affects the applicability of the second order MaxEnt model. We show that a sampling time bin of very small or very large size can lead to rather large strengths of high order interactions, thus giving rise to the failure of the second order MaxEnt model. In addition, we investigate whether weak high order correlations can explain the success of the second order MaxEnt model. We find that even when high order correlations are small, the high order interactions in the MaxEnt model can still be very large in strength, thus leading to the failure of the second order MaxEnt models. This emphasizes that the success of the second order MaxEnt model is not simply a consequence of weak correlations.

The article is organized as follows. In Section 2, the HH neuron model used in our work is recapitulated. In Section 3, we describe the basic setting for the application of the MaxEnt model in analyzing data of neuronal networks. Section 4 is devoted to the derivation of an explicit mathematical form for all the interactions of the nth order MaxEnt model with all orders of correlations as constraints. Here, we establish an important recursive relation among these different order interactions. In Section 5, we show numerically that the strengths of high order interactions in the nth order MaxEnt model are much smaller than the two leading order ones in the second order MaxEnt model in dynamical states for which the second order MaxEnt model can well approximate the distribution of neuronal firing patterns. In Section 6, we theoretically

explore a network dynamical state characterized by a linearity condition that underlies the success of the second order MaxEnt model. In Section 7, we numerically verify the linearity condition using HH neuronal network models. In Section 8, using our theoretical framework, we investigate other important issues related to the MaxEnt model. Finally, we present our conclusion in Section 9.

2. The Hodgkin–Huxley neuron model

In this work, we will use spike trains obtained from simulation of conductance-based Hodgkin–Huxley (HH) neuronal networks to demonstrate the applicability of the MEP. We process the simulation data as follows: If the ith neuron fires at least once during the sampling time bin Δt_k, whose size is usually selected to be $10\,\mathrm{ms}-20\,\mathrm{ms}$ as in experiments [34,36,41], the neuronal state σ_i is set to be 1, otherwise 0. For the total n recorded neurons, the firing pattern in each sampling time bin can be characterized by a binary vector $V=(\sigma_1,\cdots,\sigma_n)\in\{0,1\}^n$.

In the HH neuron model, for neuron i, its membrane potential V_i obeys

$$C\frac{\mathrm{d}V_i}{\mathrm{d}t}=-(V_i-V_{\mathrm{Na}})G_{\mathrm{Na}}\mathrm{h}_i\mathrm{m}_i^3-(V_i-V_{\mathrm{K}})G_{\mathrm{K}}\mathrm{n}_i^4-(V_i-V_{\mathrm{L}})G_{\mathrm{L}}+I_i^{\mathrm{input}},$$

with

$$\frac{\mathrm{d}X_i}{\mathrm{d}t}=(1-X_i)\alpha_X(V_i)-X_i\beta_X(V_i),$$

where $X\in\{\mathrm{m},\mathrm{n},\mathrm{h}\}$ and

$$\alpha_{\mathrm{n}}(V_i)=\frac{0.1-0.01V_i}{\exp(1-0.1V_i)-1},\qquad \beta_{\mathrm{n}}(V_i)=0.125\exp(-V_i/80),$$
$$\alpha_{\mathrm{m}}(V_i)=\frac{2.5-0.1V_i}{\exp(2.5-0.1V_i)-1},\quad \beta_{\mathrm{m}}(V_i)=4\exp(-V_i/18),$$
$$\alpha_{\mathrm{h}}(V_i)=0.07\exp(-V_i/20),\qquad \beta_{\mathrm{h}}(V_i)=\frac{1}{\exp(3-0.1V_i)+1}.$$

The quantities of V_i, m_i, n_i, h_i, I_i^{input} are functions of time t, and other parameters are $V_{\mathrm{Na}}=115\,\mathrm{mV}$, $V_{\mathrm{K}}=-12\,\mathrm{mV}$, $V_{\mathrm{L}}=10.6\,\mathrm{mV}$ (*i.e.,* the resting potential is set to $0\,\mathrm{mV}$), $G_{\mathrm{Na}}=120\,\mathrm{mS}\cdot\mathrm{cm}^{-2}$, $G_{\mathrm{K}}=36\,\mathrm{mS}\cdot\mathrm{cm}^{-2}$, $G_{\mathrm{L}}=0.3\,\mathrm{mS}\cdot\mathrm{cm}^{-2}$ and the membrane capacity $C=1\,\mu\mathrm{F}\cdot\mathrm{cm}^{-2}$. I_i^{input} represents external inputs and interactions between neurons,

$$I_i^{\mathrm{input}}=I_i^{\mathrm{E}}+I_i^{\mathrm{I}},\quad I_i^{\mathrm{E}}=-(V_i-V_G^{\mathrm{E}})G_i^{\mathrm{E}},\quad I_i^{\mathrm{I}}=-(V_i-V_G^{\mathrm{I}})G_i^{\mathrm{I}},$$

where I_i^{E} and I_i^{I} are excitatory and inhibitory inputs, respectively, and V_G^{E} and V_G^{I} are their corresponding reversal potentials. The conductance G_i^Q ($Q\in\{\mathrm{E},\mathrm{I}\}$) evolves according to

$$\frac{\mathrm{d}G_i^Q}{\mathrm{d}t}=-\frac{G_i^Q}{\sigma_G^Q}+H_i^Q,\quad \frac{\mathrm{d}H_i^Q}{\mathrm{d}t}=-\frac{H_i^Q}{\sigma_H^Q}+\sum_k F_i^Q\delta(t-T_{i,k}^F)+\sum_{j\neq i}S_{ij}g(V_j^{\mathrm{pre}})$$

with

$$g(V_j^{\mathrm{pre}})=1/\left(1+\exp(-(V_j^{\mathrm{pre}}-85\,\mathrm{mV})/2)\right),$$

where F_i^Q is the magnitude of an external Poisson input to neuron i, $T_{i,k}^F$ is the time of the kth input event described by a Poisson process with rate μ_i. For all the neurons

we use $F_i^{\mathrm{E}} = F$, $F_i^{\mathrm{I}} = 0$, $\mu_i = \mu$. S_{ij} is the coupling strength from the jth neuron to the ith neuron. V_j^{pre} is the membrane potential of the jth neuron (presynaptic to the ith neuron). $V_G^{\mathrm{E}} = 65\,\mathrm{mV}$, $V_G^{\mathrm{I}} = -15\,\mathrm{mV}$, $\sigma_G^E = 0.5\mathrm{ms}$, $\sigma_H^E = 3.0\mathrm{ms}$, $\sigma_G^I = 0.5\mathrm{ms}$, $\sigma_H^I = 7.0\mathrm{ms}$.

We use the adjacency matrix $A = (A_{ij})$ to denote the neuronal network structure, *i.e.*, $S_{ij} = A_{ij} S^{Q_i Q_j}$, and $S^{Q_i Q_j}$ is one of S^{EE}, S^{EI}, S^{IE}, S^{II}, depending on the type of the corresponding neuron pair (E for excitatory, I for inhibitory). $A_{ij} \neq 0$ means there is a direct coupling to the ith neuron from the jth neuron. By homogeneous coupling, we mean a statistical homogeneous architecture, that is A_{ij} equals either 1 with probability of p or 0 with probability of $1-p$. During one simulation, all the parameters are kept constant.

In our numerical simulation, we used an explicit fourth order Runge–Kutta method with time step $\sim 0.03\mathrm{ms}$. The voltage time series were obtained with a sampling rate of 2kHz. The spike train data are constructed from the voltage measurement, $x_t = 1$ if $V_i(t)$ just passes through the threshold (10mV was used) from below in voltage, $x_t = 0$ otherwise.

3. The MaxEnt model

The basic setting for the application of the MaxEnt method is as follows. For an underlying large network, a subset of neurons is recorded simultaneously. For the total n recorded neurons, the firing pattern in each sampling time bin can be characterized by a binary vector $V = (\sigma_1, \cdots, \sigma_n)$. In general, to obtain the distribution of V requires to know all the possible states of V, *i.e.*, 2^n states in total. The distribution of the 2^n states can be determined by correlations of all orders and the normalization of probability. The expected value of σ_i is given by $\bar{\sigma}_i = \langle \sigma_i \rangle_E$, where $\langle \cdot \rangle_E$ is defined by

$$\langle g(t) \rangle_E = \frac{1}{N_T} \sum_{t=1}^{N_T} g(t)$$

for any function $g(t)$ and N_T is the total number of sampling time bins in the recording. The second order correlation is given by $\langle (\sigma_i - \bar{\sigma}_i)(\sigma_j - \bar{\sigma}_j) \rangle_E$ for $i \neq j$. Similarly, higher order correlations can be evaluated. To obtain correlations up to the mth order requires to evaluate all $\langle \sigma_{i_1} \cdots \sigma_{i_M} \rangle_E$, where $i_1 < i_2 < \cdots < i_M$ and $1 \leq M \leq m$.

The entropy of the firing pattern of neurons is defined by

$$S = -\sum_V P(V) \log P(V),$$

where $P(V)$ is the probability of the state V in all sampling time bins. The MEP is to find the desired probability distribution for n neurons by maximizing the entropy S subject to given correlations up to the mth order ($m \leq n$) [34, 36, 41]. Then, the unique distribution can be solved as

$$P_m(V) = \frac{1}{Z} \exp\Big(\sum_{i_1=1}^{n} J_{i_1} \sigma_{i_1} + \sum_{i_1 < i_2}^{n} J_{i_1 i_2} \sigma_{i_1} \sigma_{i_2} \cdots + \sum_{i_1 < \cdots < i_m}^{n} J_{i_1 \cdots i_m} \sigma_{i_1} \cdots \sigma_{i_m} \Big), \qquad (3.1)$$

where, following the terminology of statistical physics, the first order interaction J_i is the self interaction, $J_{i_1 \cdots i_k}$ is the kth order interaction ($2 \leq k \leq m$), the partition function Z is the normalization factor. Equation (3.1) is referred to as the distribution of the mth order MaxEnt model. Note that the distribution of the nth order MaxEnt model P_n is estimated under the constraints of the correlations up to the nth order, it can be shown

that P_n is identical to $P(V)$ [41]. For P_m with $m<n$, we use the same iteration method as in [41] to numerically solve the above MaxEnt optimization problem to obtain the interaction parameters and the corresponding distribution (See Appendix for details.). We denote the entropy corresponding to the mth order MaxEnt Model P_m as

$$S_m = -\sum_V P_m(V)\log P_m(V). \tag{3.2}$$

Because increasing number of correlation constraints always reduces entropy, it can be easily seen that $S_1 \geq S_2 \geq \cdots \geq S_n = S$ [36, 41], where S is the entropy that satisfies all correlation constraints up to the nth order. From information theory [34], multi-information is defined as $I_n = S_1 - S_n$. The amount of information accounted for by the second order information is $I_2 = S_1 - S_2$. The multi-information fraction is therefore defined by

$$g_I = \frac{I_2}{I_n}, \tag{3.3}$$

which is commonly used to index the performance of the second order MaxEnt model [2, 23, 29, 34, 36, 41, 45, 48]. Another closely related multi-information fraction has also been used to index the performance of the MaxEnt model [41], that is,

$$f_I = \frac{D_1 - D_2}{D_1}, \tag{3.4}$$

where D_m is the Kullback–Leibler (KL) divergence of P_n with respect to P_m given by

$$D_m = \sum_V P_n(V)\log\frac{P_n(V)}{P_m(V)}. \tag{3.5}$$

The indexes [Equations (3.3) and (3.4)] are unity only when the distribution of the nth order MaxEnt (the observed distribution), *i.e.*, P_n, is exactly the same as the distribution of the second order MaxEnt model. Our results show that the conclusions using f_I and g_I are similar. For brevity, we only show the results using f_I below. The value of multi-information fraction f_I is found to be in the range of $90\% - 99\%$ for various states of the brain in experiments, for example, the spontaneous state [36, 41] or the state under the visual-input drive [34].

We further note that in the following we will use the KL divergence of P_n with respect to P_1, *i.e.*, D_1, as a synchronization index. If the activities of neurons are totally independent, *i.e.*, in the most asynchronous state, $D_1 = 0$ since the joint distribution in such case is simply the product of the marginal distribution of each neuron.

4. Analytical solutions to interactions in the nth order MaxEnt model

As mentioned above, if we use the MaxEnt model of less than the nth order to fit the distribution of neuronal firing patterns of n neurons in a network, we can use an iteration method to numerically obtain the corresponding interaction strengths. In this section, we will show that the interaction strengths of the nth order MaxEnt model can be analytically solved.

For a fixed sampling time bin, we partition the recording time by the bin size and record the state of neurons at every sampling time bin. A binary vector $V = (\sigma_1, \sigma_2, \cdots, \sigma_n) \in \{0,1\}^n$ then represents the state of n neurons. We count the occurring frequency of all possible states as the observed distribution $P(V)$ of neuronal firing

patterns. As discussed in the previous section, P_n is identical to $P(V)$ for the nth order MaxEnt model. Substituting 2^n states of $V=(\sigma_1,\sigma_2,\cdots,\sigma_n)$ and the observed probability $P(V)$ of the state V of n neurons into the nth order MaxEnt model [Equation (3.1)], then taking the logarithm of both sides of Equation (3.1), we obtain a system of linear equations for all the interactions in terms of $P(V)$,

$$\sum_{i_1=1}^{n} J_{i_1}\sigma_{i_1}+\sum_{i_1<i_2}^{n} J_{i_1 i_2}\sigma_{i_1}\sigma_{i_2}\cdots+J_{12\cdots n}\sigma_1\sigma_2\cdots\sigma_n=\log P(V)+\log Z, \tag{4.1}$$

where $J_{i_1\cdots i_m}$ are the mth order interactions in P_n. Note that the partition function $Z=1/P(V=(0,0,\cdots,0))$. By solving the system of linear equations [Equation (4.1)], we can obtain all the 2^n-1 interactions J's for the nth order MaxEnt model in terms of $P(V)$.

Using $n=3$ as an example, by denoting $P_{\sigma_1\cdots\sigma_n}$ as the probability of state $V=(\sigma_1,\cdots,\sigma_n)$, we have

$$J_1=\log\frac{P_{100}}{P_{000}} \tag{4.2}$$

and the second order interaction is

$$J_{12}=\log\frac{P_{110}}{P_{010}}-\log\frac{P_{100}}{P_{000}}. \tag{4.3}$$

Note that J_{12} can be equivalently obtained by the following procedure: First, in $J_1=\log(P_{100}/P_{000})$, we switch the state of the second neuron from silence to active to obtain a new term $\log(P_{110}/P_{010})$. Then, we subtract J_1 from the new term to obtain J_{12}. This procedure can be extended to the case of higher orders:

THEOREM 4.1. *For a network of n neurons, in the nth order MaxEnt model, the $(k+1)$st order interaction $J_{123\ldots(k+1)}$ can be obtained as follows: First, we switch the state of the $(k+1)$st neuron in $J_{123\ldots k}$ from silence to active to obtain a new term $J^1_{123\ldots k}$. Then, we subtract $J_{123\ldots k}$ from the new term to obtain $J_{123\ldots(k+1)}$, i.e.,*

$$J_{123\ldots(k+1)}=J^1_{123\ldots k}-J_{123\ldots k}. \tag{4.4}$$

Proof. Defining U^l_m as

$$U^l_m=\sum_{V\in S^l_m}\log P(V), \tag{4.5}$$

in which $S^l_m=\{(\sigma_1,\sigma_2,\cdots,\sigma_n)|\sum_{i=1}^m\sigma_i=l;\sigma_j=0,m<j\le n\}$, $0\le l\le m\le n$, we show below that the interaction can be expressed in terms of U^l_m, specifically, the kth order interaction $J_{12\cdots k}$ can be written as

$$J_{12\cdots k}=\sum_{i=0}^{k}(-1)^{k-i}U^i_k. \tag{4.6}$$

For an arbitrary kth order interaction $J_{i_1\cdots i_k}$, we can use another index order set to denote the neurons, *i.e.*, $\{i_1,i_2,\cdots,i_n\}$, which is a permutation of $\{1,2,\cdots,n\}$ by $g\to i_g$ for $1\le g\le n$. Therefore, if Equation (4.6) is valid, then we have

$$J_{i_1\cdots i_k}=\sum_{i=0}^{k}(-1)^{k-i}U^i_{A_k} \tag{4.7}$$

where $A_k = \{i_1, \cdots, i_k\}$,

$$U^l_{A_k} = \sum_{V \in S^l_{A_k}} \log P(V)$$

and $S^l_{A_k} = \{(\sigma_{i_1}, \sigma_{i_2}, \cdots, \sigma_{i_n}) | \sum_{i_g \in A_k} \sigma_{i_g} = l; \sigma_{i_g} = 0, k < g \leq n\}$. Note that S^l_k is a special case of $S^l_{A_k}$.

Equation (4.6) can be proven by mathematical induction. For $k=1$, substituting the state $V = (1,0,0,\cdots,0)$ and $P_{100\cdots0}$ into the nth order MaxEnt model (4.1), we have

$$\begin{aligned} J_1 &= \log P_{100\cdots0} - \log P_{000\cdots0} \\ &= U^1_1 - U^0_1. \end{aligned}$$

Therefore, Equation (4.6) holds for $k=1$. Assuming Equation (4.6) holds for all integers no larger than k and substituting $V = (1,1,\cdots,1,0,\cdots,0)$ (neurons from 1 to $k+1$ are active and neurons from $k+2$ to n are silent) into the nth order MaxEnt model (3.1), we obtain

$$J_{1\cdots(k+1)} + \sum_{g=1}^{k} \sum_{i_1 < \cdots < i_g}^{k+1} J_{i_1 \cdots i_g} = U^{k+1}_{k+1} - U^0_{k+1}. \tag{4.8}$$

The reason of why there are no terms of order higher than $k+1$ is that there are only $k+1$ neurons firing. For $g \leq k$, from Equations (4.6) and (4.7), by induction assumption we have

$$\sum_{i_1 < \cdots < i_g}^{k+1} J_{i_1 \cdots i_g} = \sum_{i=0}^{g} (-1)^{g-i} C^{g-i}_{k+1-i} U^i_{k+1}, \tag{4.9}$$

where C^{g-i}_{k+1-i} comes from the selection of $g-i$ terms from all the possible $k+1-i$ choices for a given i. Since $J_{i_1 \cdots i_g}$ is the gth order interaction, as is in Equation (4.7), the sign of the logarithm probability of a state in which there are i neurons firing is $(-1)^{g-i}$. For a pair of given g and i, we want to count how many times of $(-1)^{g-i} U^i_{k+1}$ occurring on the left hand side of Equation (4.9). Every state V of S^i_{k+1} occurs once in the summation terms of U^i_{k+1} in Equation (4.5). To count the number of occurrence of $(-1)^{g-i} U^i_{k+1}$, we can count the number of occurrence of an element of S^i_{k+1}, denoted by V_c, in which the state of a neuron is active if its index belongs to $Q_s = \{j_1, j_2, \cdots, j_i\}$. For the given g, we would select a subset D of g elements from $\{1,2,\cdots,k+1\}$ for the indexes $\{i_1, \cdots, i_g\}$ for every summation term on the left hand side of Equation (4.9). If $Q_s \subseteq D$, then, from Equation (4.7), $\log P(V_c)$ would occur once in $J_{i_1 \cdots i_g}$. To count the number of occurrence of $\log P(V_c)$, we need to count how many subsets D containing Q_s. Since there are i elements of D belonging to Q_s, we still need to select $g-i$ elements from $k+1-i$ elements for D. This number of selection is C^{g-i}_{k+1-i}. Hence, the coefficient of $(-1)^{g-i} U^i_{k+1}$ is C^{g-i}_{k+1-i}. Then, we have

$$J_{1\cdots(k+1)} = U^{k+1}_{k+1} - U^0_{k+1} - \sum_{g=1}^{k} \sum_{i=0}^{g} (-1)^{g-i} C^{g-i}_{k+1-i} U^i_{k+1}. \tag{4.10}$$

The coefficient of U^0_{k+1} is

$$-1 - \sum_{g=1}^{k} (-1)^g C^g_{k+1} = (-1)^{k+1}. \tag{4.11}$$

For $k+1>l>0$, the coefficient of U^l_{k+1} is

$$-\sum_{g=l}^{k}(-1)^{g-l}C^{g-l}_{k+1-l}=(-1)^{k+1-l}. \tag{4.12}$$

Combining Equations (4.10), (4.11) and (4.12), we arrive at

$$J_{1\cdots(k+1)}=\sum_{i=0}^{k+1}(-1)^{k+1-i}U^i_{k+1}, \tag{4.13}$$

i.e., Equation (4.6) is valid by induction for $1\le k\le n$.

Based on Equation (4.6), we now show the validity of Equation (4.4). For $1\le i\le k$, there are i neurons out of $k+1$ neurons firing in the states described by U^i_{k+1} of S^i_{k+1}. For $i<k+1$, we can split U^i_{k+1} into two terms, one is U^i_k, where the $(k+1)$st neuron is silent, the other term is $V^{i-1}_k\equiv U^i_{k+1}-U^i_k$, where the $(k+1)$st neuron is active. By defining $V^k_k\equiv U^{k+1}_{k+1}$, from Equation (4.13), we have

$$\begin{aligned}
J_{1\cdots(k+1)}&=U^{k+1}_{k+1}-U^k_{k+1}+U^{k-1}_{k+1}+\cdots.\\
&=V^k_k-(V^{k-1}_k+U^k_k)+(V^{k-2}_k+U^{k-1}_k)+\cdots\\
&=[V^k_k+\cdots+(-1)^{k-i}V^{k-i}_k+\cdots+(-1)^kV^0_k]\\
&\quad-[U^k_k+\cdots+(-1)^{k-i}U^{k-i}_k+\cdots+(-1)^kU^0_k]\\
&=J^1_{12\cdots k}-J_{12\cdots k},
\end{aligned}$$

where $J^1_{12\cdots k}$ is a new quantity which switches the state of the $(k+1)$st neuron from silence to active in $J_{123\ldots k}$. This is the conclusion in Equation (4.4). □

To illustrate, for example, for $n=4$, we have

$$J_{12}=\log\frac{P_{1100}}{P_{0100}}-\log\frac{P_{1000}}{P_{0000}}$$

and

$$J_{123}=\left(\log\frac{P_{1110}}{P_{0110}}-\log\frac{P_{1010}}{P_{0010}}\right)-\left(\log\frac{P_{1100}}{P_{0100}}-\log\frac{P_{1000}}{P_{0000}}\right). \tag{4.14}$$

Using this method, $J_{123\ldots k}$ for any $k\le n$ can be decomposed into 2^{k-1} terms, where every term can be interpreted as the logarithmic probability ratio of the active to the inactive state of the first neuron while keeping the state of other neurons unchanged. In the following, we will refer to such a term as a fundamental term as the following

$$\text{A fundamental term: } \log\frac{P_{1,\sigma_2,\sigma_3,\cdots,\sigma_n}}{P_{0,\sigma_2,\sigma_3,\cdots,\sigma_n}}, \tag{4.15}$$

where $P_{1,\sigma_2,\sigma_3,\cdots,\sigma_n}$ and $P_{0,\sigma_2,\sigma_3,\cdots,\sigma_n}$ are the probabilities that neuron 1 is spiking and silent, respectively, while the states of other neurons are $\sigma_2,\sigma_3,\cdots,\sigma_n$, respectively. For example, in J_{123}, a fundamental term of the first neuron is $\log(P_{1010}/P_{0010})$ as shown in Equation (4.14), which is the logarithmic probability ratio of the active to the inactive state of the first neuron under the condition that the second and the fourth neuron stay silent and the third neuron is active.

5. Weak high order interactions

For a network of n neurons, there are 2^n possible firing states. To obtain the distribution of the firing patterns, one way is to measure the probabilities of 2^n firing states from recorded data. Another way is to acquire all correlations of all the orders (There are 2^n-1 such correlations including the mean values of σ_i for $1\leq i\leq n$.). Combining with the normalization of the probability, we have 2^n conditions (constraints). The distribution P_n produced by the nth order MaxEnt model is estimated under the constraints of the correlations up to the nth order, one can show that the distribution P_n is identical to the observed distribution of neuronal firing patterns [41]. When not all order correlations are constrained, we need to address the question of why a low order (less than nth order) MaxEnt model can well approximate the observed distribution of neuronal firing patterns. For example, the second order MaxEnt model has been commonly used. A possible underlying reason may be that high order interactions of the nth order MaxEnt model P_n are much smaller than the two leading order ones.

Since we are able to obtain the interaction strengths of the nth order MaxEnt model from the observed distribution as discussed in Section 4, we first examine the magnitude of interaction strengths in numerical experiments to see whether the above supposition is true. Figure 5.1A displays an example of interactions of various orders versus the sampling time bin size. The data is from a homogeneously coupled HH neuronal network of 5 neurons driven by a Poisson input. The mean interspike interval of each neuron is 47 ms. We record the spike trains of all five neurons for the duration of 1.4×10^6 s, which is sufficiently long to reliably obtain a stable distribution of neuronal firing patterns. The interaction strengths are obtained from the observed distribution using Equations (4.6) and (4.7). For the given sampling time bin size, the average kth order interaction strength is computed as the mean absolute value of interaction strengths of the corresponding order. We examine different bin sizes, ranging from 9 ms to 81 ms, to make sure the robustness of our analysis. In Figure 5.1A, the magenta line is for the interactions of the self interaction (first order), green for the second order, red for the third order, blue for the fourth order, cyan for the fifth order interactions and the black solid line is for the multi-information fraction f_I. It can be seen clearly that the average strength of interactions of higher order is at least one order of magnitude smaller (in the absolute value) than the two leading orders, and the multi-information fraction f_I is $\sim$99.8%. As shown in Figure 5.1B, for all the bin sizes, the predicted distributions of the second order MaxEnt model P_2 (blue) are in excellent agreement with the observed distributions while the distribution of the first order MaxEnt model P_1 (green) deviates substantially from the observed distributions.

From our numerical results, we can conclude that the strengths of high order interactions are much smaller than the first and second order interactions when the second order MaxEnt model can well approximate the distribution of neuronal firing patterns. Therefore, the weak high order interactions in MaxEnt models may underly the fact that the second order MaxEnt model can be a good effective description as signified by f_I being very close to unity. In the following, we will theoretically analyze under what condition strengths of high order interactions of the nth order MaxEnt model can be significantly smaller than the low order ones and whether under this condition one can theoretically show that a second order MaxEnt model can well approximate the observed distributions.

6. A dynamical network state underlying the second order MaxEnt Model

In this section, we address the question of under what condition the strengths of

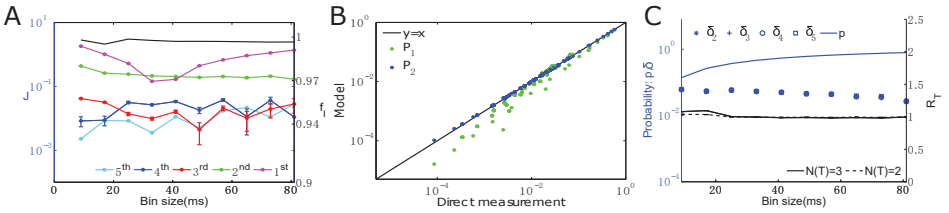

FIG. 5.1. **Numerical results of neuronal networks.** *The simulation is for a network of five excitatory HH neurons with all-to-all connections. The coupling strength is* $s=0.0714\,\mathrm{ms}^{-1}$ *(The corresponding physiological excitatory postsynaptic potential is* $\sim 1\,\mathrm{mV}$*). The input parameters are chosen as* $\mu=1\,\mathrm{ms}^{-1}$ *(Poisson input rate) and* $f=0.035\,\mathrm{ms}^{-1}$ *(Poisson input magnitude). The mean interspike interval is* 47 ms*. The total recording time is* 1.4×10^6 s*. All* 5 *neurons are selected to carry out the MaxEnt model analysis. (A) The black line (the right ordinate) is the multi-information fraction; Colored lines (the left ordinate) correspond to different orders of interactions. The data point is the mean absolute value of interaction strengths of the corresponding order for different sampling time bin sizes, the first order (magenta), the second order (green), the third order (red), the fourth order (blue), and the fifth order (cyan). The standard deviation is also indicated by the error bar around the mean and it is generally rather small. (B) The rate of occurrence of each firing state predicted from the distribution of the second order MaxEnt model* P_2 *(blue) and the distribution of the first order MaxEnt model* P_1 *(green) is plotted against the measured occurrence rate generated from the numerical simulation, the data of all bin sizes are plotted. (C) The solid blue line (the left ordinate) is the conditional probability* p *of neuron* 1 *in the active state conditioned on other neurons being silent for different sampling time bins. Blue asterisks, plus signs, circles, and squares (the left ordinate) are the values of the probability increment of neuron* 1 *in the active state caused by neuron with index* $i=2,3,4,5$ *(*δ_i*), respectively.* δ_i *for* $i=2,3,4,5$ *overlaps one another well, which is a consequence of homogeneity. The dashed and solid black lines (the right ordinate) are the mean values of* R_T *[Equation (6.9)] for all subsets* T *with size* $N(T)=2,3$*, respectively. The standard deviation is also indicated around the mean and it is rather small with the error bars below the line width (The maximum value of all standard deviations is less than* 0.03*).*

high order (above second order) interactions in the MaxEnt model can be much smaller than the low order ones. For illustration, we first consider a homogeneously coupled network of three neurons with all-to-all connections (no self connections). By symmetry, without loss of generality, we can select neuron 1 and consider the following quantities:

$$p=P(\sigma_1=1|\sigma_2=0,\sigma_3=0), \tag{6.1}$$

$$\delta_2=P(\sigma_1=1|\sigma_2=1,\sigma_3=0)-p, \tag{6.2}$$

$$\delta_3=P(\sigma_1=1|\sigma_2=0,\sigma_3=1)-p, \tag{6.3}$$

$$p+\delta_2+a\delta_3=P(\sigma_1=1|\sigma_2=1,\sigma_3=1), \tag{6.4}$$

where p is the conditional probability that neuron 1 is spiking while other neurons are silent, δ_i is the increment of conditional probability of the first neuron in the active state induced by the ith neuron on spiking while others are silent, where $i=2,3$. For example, $p+\delta_2$ is the probability that the first neuron spikes conditioned on the second neuron's firing while the third neuron being silent. By homogeneity, we have $\delta_i=\delta$. The parameter a in Equation (6.4) is used to characterize how linear the neuronal system is in the following sense: If $a=1$, the conditional probability increment of the first neuron in the active state induced by neurons 2 and 3 is equal to the sum of increments separately induced by each individual neuron, *i.e.*,

$$P(\sigma_1=1|\sigma_2=1,\sigma_3=1)=p+\delta_2+\delta_3.$$

When this condition holds, we refer to the network dynamical state of the system as being linear. In numerical simulation, we observe that, when the neuronal dynamics is not too synchronized, δ is very small compared to the value of the conditional probability p. As shown in Equation (6.2), δ_i can be computed from conditional probabilities of the observed distribution. For example, in the numerical example as shown in Figure 5.1C, when the sampling time bin size is larger than 30ms, δ_i (blue asterisks, plus signs, circles and squares for $i=2,3,4,5$, respectively.) are one order of magnitude smaller than the conditional probability p (blue line). Incidentally, we note that as a consequence of homogeneity, δ_i induced by different neuron i overlaps one another well in Figure 5.1C. In the following, we assume that δ is sufficiently small and perform a perturbative analysis of interactions with respect to δ. As discussed above, we can write the interaction J_{12} in terms of conditional probabilities

$$J_{12}=\log\frac{P(\sigma_1=1|\sigma_2=1,\sigma_3=0)}{P(\sigma_1=0|\sigma_2=1,\sigma_3=0)}-\log\frac{P(\sigma_1=1|\sigma_2=0,\sigma_3=0)}{P(\sigma_1=0|\sigma_2=0,\sigma_3=0)}. \tag{6.5}$$

For $\delta\ll p$, by using Equations (6.1) and (6.2), and performing a Taylor expansion, Equation (6.5) becomes

$$J_{12}=\frac{1}{(1-p)p}\delta+o(\delta), \tag{6.6}$$

in which $o(\cdot)$ symbol stands for higher order terms. Similarly, using Equations (6.1)–(6.4), we have

$$J_{123}=\frac{2-(1+a)}{(p-1)p}\delta+\frac{[2-(1+a)^2](1-2p)}{2(p-1)^2p^2}\delta^2+o(\delta^2). \tag{6.7}$$

Under the condition of linearity, *i.e.*, $a=1$, Equation (6.7) simplifies to

$$J_{123}\sim\frac{2p-1}{(1-p)^2p^2}\delta^2. \tag{6.8}$$

For this three neuron case, therefore, we have $J_{12}=\mathcal{O}(\delta)$ and $J_{123}=\mathcal{O}(\delta^2)$ under the linearity condition. We will show below that this ordering can be extended to high order interactions. First, we extend the linearity condition $a=1$ to a neuronal group of large size. We denote

$$p=P(\sigma_1=1|\sigma_j=0,j\in S),$$

$$\delta_i=P(\sigma_1=1|\sigma_i=1,\sigma_j=0,j\in S\backslash\{i\})-p,$$

in which $S=\{2,3,\cdots,n\}$. We use the following index to characterize how linear the system is:

$$R_T=\frac{P(\sigma_1=1|\sigma_j=1,j\in T;\sigma_k=0,k\in S\backslash T)}{p+\sum_{i\in T}\delta_i}, \tag{6.9}$$

where n is the number of neurons in the selected group, T is any subset of S. If R_T is unity for any subset T, we say that the linearity condition holds for the neuronal network dynamics. Based on the linearity condition, we analyze the interactions and multi-information fraction as follows.

6.1. Perturbative analysis of interactions. Now we are ready to demonstrate that in general the interaction strengths of the nth order MaxEnt model form a hierarchy in the power of δ under the linearity condition. In a homogeneous network of n neurons with all-to-all connections, under the linearity condition, as defined in Equation (6.9), for the first neuron, a fundamental term (4.15) of m other neurons that fire (Here, we refer the other neurons as the neurons whose indexes belong to $S=\{2,3,\cdots,n\}$.) is

$$G_p(m) \equiv \log \frac{p+m\delta}{1-(p+m\delta)}. \tag{6.10}$$

For example, $m=1$, $n=3$, we have

$$\begin{aligned}\log \frac{P_{110}}{P_{010}} &= \log \frac{P(\sigma_1=1|\sigma_2=1,\sigma_3=0)}{P(\sigma_1=0|\sigma_2=1,\sigma_3=0)}\\ &= \log \frac{p+\delta}{1-(p+\delta)}\\ &= G_p(1).\end{aligned}$$

THEOREM 6.1. *For a network of n neurons, assuming $\delta_i=\delta$, under the linearity condition, the kth order interaction $J_{123\ldots k}$ of the nth order MaxEnt model (3.1) satisfies the following relation,*

$$J_{12\cdots k} = \mathcal{O}(\delta^{k-1}). \tag{6.11}$$

Proof. As seen in Equations (6.6) and (6.8), under the linearity condition, $J_{12}\sim \mathcal{O}(\delta)$ and $J_{123}\sim\mathcal{O}(\delta^2)$, *i.e.*, Equation (6.11) holds for $k=1,2$. Next, we assume that Equation (6.11) holds for some k, where $n>k\geq 1$. Just like J_{123} in Equation (4.14), the kth order interaction can be expressed by a linear combination of the fundamental terms. Since under the linearity condition, a fundamental term of m other neurons firing is the same as $G_p(m)$ in Equation (6.10) , which is an elementary function of p and δ, $J_{12\cdots k}$ can be expressed as a combination of elementary functions of p and δ. By the induction assumption, $J_{123\ldots k}$ is $\mathcal{O}(\delta^{k-1})$, then, we can denote $J_{12\cdots k}$ with respect to δ as $J_{12\cdots k}=W_k(p)\delta^{k-1}+\mathcal{O}(\delta^k)$, where $W_k(p)$ is a differentiable function with respect to $p\in(0,1)$.

Through Theorem (4.1), to compute $J_{123\ldots(k+1)}$, we first need to compute a new quantity $J^1_{123\ldots k}$, which switches the state of the $(k+1)$st neuron from silence to active in $J_{123\ldots k}$. Under the linearity condition, after we switch the state of the $(k+1)$st neuron, the fundamental term, where there are m other neurons firing, becomes a fundamental term of $m+1$ other neurons firing, that is,

$$G_p(m) = \log \frac{p+m\delta}{1-(p+m\delta)} \to \log \frac{p+(m+1)\delta}{1-[p+(m+1)\delta]} \tag{6.12}$$

$$= \log \frac{(p+\delta)+m\delta}{1-[(p+\delta)+m\delta]} \tag{6.13}$$

$$= G_{p+\delta}(m), \tag{6.14}$$

which is also equivalent to switching p in the fundamental terms of $J_{123\ldots k}$ to $p+\delta$ while keeping m other neurons in the firing state. For $\delta \ll p$, the leading term of $J^1_{123\ldots k}$ is as follows

$$W_k(p+\delta)\delta^{k-1} = W_k(p)\delta^{k-1} + \frac{dW_k}{dp}\delta^k + \mathcal{O}(\delta^{k+1}).$$

Hence, the leading order terms of $J^1_{123\ldots k}$ and $J_{123\ldots k}$ have exactly the same form. From Theorem (4.1), we can see that $J_{123\ldots(k+1)}$ is at least one order higher than $J_{123\ldots k}$ with respect to δ. Therefore, by induction, Equation (6.11) holds for interactions of any order. ∎

REMARK 6.1. For a nonhomogeneous case, under the linearity condition, after we switch the state of the $(k+1)$st neuron, a fundamental term in $J_{123\ldots k}$ in which there are m other spiking neurons, whose indexes are denoted as i_j, where $j=1,2,\cdots m$, $2\le i_j\le k$ and $i_{j_1}\neq i_{j_2}$ for $j_1\neq j_2$, is changed as follows,

$$\log\frac{p+\sum_{j=1}^m c_{i_j}\delta_{max}}{1-(p+\sum_{j=1}^m c_{i_j}\delta_{max})}\to\log\frac{(p+\delta_{k+1})+\sum_{j=1}^m c_{i_j}\delta_{max}}{1-[(p+\delta_{k+1})+\sum_{j=1}^m c_{i_j}\delta_{max}]},$$

where $\delta_{max}=\max_{1\le i\le n}\delta_i$, c_i is defined by $\delta_i=c_i\delta_{max}$ for $1\le i\le n$. Hence, this is also equivalent to switching p in the fundamental terms of $J_{123\ldots k}$ to $p+c_{k+1}\delta_{max}$ while keeping m other neurons in the firing state. If $\delta_{max}\ll p$, we can obtain similar results, *i.e.*, the strengths of interactions also form a hierarchy in the power of δ_{max}.

From Theorem (6.1), we can derive the exact form of the leading order terms of $J_{123\ldots k}$ with respect to δ. To see this, we first introduce the following lemma:

LEMMA 6.1. *For a network of n neurons, assuming $\delta_i=\delta$, under the linearity condition, the kth order interaction $J_{123\ldots k}$ of the nth order MaxEnt model (3.1) satisfies the following relation,*

$$J_{123\ldots k}=\sum_{m=0}^{k-1}(-1)^{k-m-1}C^m_{k-1}G_p(m), \tag{6.15}$$

where $k\le n$.

Proof. For any fixed n, when $k=1$,

$$\begin{aligned}J_1&=\log\frac{P_{10\cdots0}}{P_{00\cdots0}}\\&=\log\frac{p}{1-p}\\&=G_p(0),\end{aligned}$$

which demonstrates that Equation (6.15) is valid for $k=1$. We assume that Equation (6.15) holds for some k, $n>k\ge1$. If we switch the state of the $(k+1)$st neuron from silence to active, $G_p(m)$ would turn to be $G_p(m+1)$. From Equation (4.4) in Theorem (4.1) and also Equation (6.15), we have

$$\begin{aligned}J_{123\ldots(k+1)}&=\sum_{m=0}^{k-1}(-1)^{k-m-1}C^m_{k-1}G_p(m+1)-J_{123\ldots k}\\&=\sum_{m=0}^{k-2}G_p(m+1)\left[C^m_{k-1}(-1)^{k-m-1}-C^{m+1}_{k-1}(-1)^{k-m-2}\right]\\&\quad-G_p(0)(-1)^{k-1}+G_p(k).\end{aligned}$$

Using $C^m_{k-1}+C^{m+1}_{k-1}=C^{m+1}_k$, we can obtain

$$J_{123\ldots(k+1)}=\sum_{m=0}^{k-2}(-1)^{k-m-1}G_p(m+1)C^{m+1}_k-(-1)^{k-1}G_p(0)+G_p(k)$$

$$= \sum_{m=0}^{k} (-1)^{k-m} C_k^m G_p(m).$$

Therefore, Equation (6.15) holds for $k+1$. By induction, Equation (6.15) is valid for any $k \leq n$. ∎

Now we can consider the leading order term of $J_{12\cdots k}$ with respect to δ. When there are m other neurons firing, the fundamental term can be easily written as

$$G_p(m) = \log\lambda + g_p(m,\delta), \tag{6.16}$$

where $\lambda = p/(1-p)$ and

$$g_p(m,\delta) \equiv \log\frac{p+m\delta}{p-m\lambda\delta}.$$

We note that

$$g_p(m,\delta) = \sum_{i=1}^{\infty} \frac{m^i}{i}[(-1)^{i+1} + \lambda^i]\left(\frac{\delta}{p}\right)^i.$$

From Equation (6.15) in Lemma (6.1), we have

$$J_{123\cdots k} = \sum_{m=0}^{k-1} (-1)^{k-m-1} C_{k-1}^m [\log\lambda + g_p(m,\delta)],$$

since $g_p(0,\delta) = 0$ and $\sum_{m=0}^{k-1}(-1)^{k-m-1}C_{k-1}^m = 0$ for $k > 1$, we can obtain

$$J_{123\cdots k} = \sum_{m=1}^{k-1} (-1)^{k-m-1} C_{k-1}^m g_p(m,\delta) \quad \text{for } k > 1.$$

By Theorem (6.1), $J_{123\cdots k}$ is $\mathcal{O}(\delta^{k-1})$. To obtain the exact form of the leading order term of $J_{123\cdots k}$, we only need to consider the terms that are of $\mathcal{O}(\delta^{k-1})$ in the fundamental terms of $J_{123\cdots k}$, this yields

$$J_{123\cdots k} = B_k[(-1)^k + \lambda^{k-1}]\left(\frac{\delta}{p}\right)^{k-1} + o\left(\delta^{k-1}\right), \tag{6.17}$$

where $k > 1$ and

$$B_k = \frac{1}{k-1}\sum_{m=1}^{k-1} (-1)^{k-m-1} C_{k-1}^m m^{k-1}.$$

Note that $J_{123\cdots k}$ in Equation (6.17) is independent of n.

6.2. Perturbative analysis of the multi-information fraction. We can also use the same framework to perform a perturbative analysis of the multi-information fraction.

THEOREM 6.2. *For a network of n neurons, under the linearity condition, if $\delta_{max} \ll p$, where $\delta_{max} = \max_i \delta_i$, we have*

$$1 - f_I \sim \mathcal{O}(\delta_{max}^2).$$

Proof. For the state of n neurons $V=(\sigma_1,\sigma_2,\cdots,\sigma_n)$ within a network, the corresponding KL divergence of $P_n(V)$ with respect to $P_m(V)$ in Equation (3.5) is

$$D_{KL}(P_n|P_m)=\sum_V P_n(V)\log\frac{P_n(V)}{P_m(V)}.$$

From Equation (3.4), we have

$$f_I=1-\frac{D_{KL}(P_n|P_2)}{D_{KL}(P_n|P_1)}. \tag{6.18}$$

Our proof is based on a perturbation expansion of the distribution $P_n(V)$ in Equation (3.1) [29]. For n neurons in a network, as discussed previously, the observed distribution $P_{obs}(V)$ is identical to the distribution of the nth order MaxEnt model subject to all 2^n-1 correlation constraints, *i.e.*, $P_{obs}(V)=P_n(V)$. When the interaction strengths from the second to the nth order in Equation (3.1) are small quantities comparing to the first order, we can perform a perturbative analysis with respect to those small components by Sarmanov–Lancaster expansion [19, 20, 33]. Under the linearity condition, when $\delta_{max}\ll p$, through Theorem (6.1), we know the strengths of high order interactions are at least one order of magnitude smaller than the first order interaction. We therefore follow the procedure of the Sarmanov–Lancaster expansion for P_{obs} as in [29]:

$$P_{obs}(V)=(1+\xi^p(V))P_{ind}(V), \tag{6.19}$$

where

$$P_{ind}(V)=\frac{\exp(\sum_j J_j^p\sigma_j)}{\Pi_j[1+\exp(J_j^p)]}, \tag{6.20}$$

$$\xi^p\equiv\sum_{i<j}^{n}J_{ij}^p\Delta\sigma_i\Delta\sigma_j+\sum_{i<j<k}^{n}J_{ijk}^p\Delta\sigma_i\Delta\sigma_j\Delta\sigma_k+h.o.t.,$$

where $\Delta\sigma_j=\sigma_j-\langle\sigma_j\rangle_{ind}$, $\langle\cdot\rangle_{ind}$ is the average with respect to $P_{ind}(V)$, *h.o.t.* stands for high order terms of interactions. The superscript p represents the fact that the parameters are those from the observed distribution $P_{obs}(V)$ as written in the form of Equation (3.1).

For any j, we denote $\bar{\sigma}_j$ as the expected value of σ_j with respect to $P_{obs}(V)$,

$$\begin{aligned}\bar{\sigma}_j=\langle\sigma_j\rangle_n&=\sum_V(1+\xi^p(V))P_{ind}(V)\sigma_j\\&=\langle\sigma_j\rangle_{ind}+\langle\xi^p(V)\sigma_j\rangle_{ind},\end{aligned} \tag{6.21}$$

where $\langle\cdot\rangle_m$ is the average with respect to $P_m(V)$ and we have $P_n(V)=P_{obs}(V)$. Since σ_i and σ_j, $i\neq j$, are independent under P_{ind} and

$$\langle\Delta\sigma_k\rangle_{ind}=0\qquad\text{for}\quad k=1,2,\cdots n. \tag{6.22}$$

To consider $\langle\xi^p(V)\sigma_j\rangle_{ind}$, we can first take a look at an example, $\langle J_{il}^p\Delta\sigma_i\Delta\sigma_l\sigma_j\rangle_{ind}$ for $i\neq l$. Since at least one of the indexes i or l is not equal to index j, say, $j\neq i$, then we have

$$\langle J_{il}^p\Delta\sigma_i\Delta\sigma_l\sigma_j\rangle_{ind}=\langle J_{il}^p\Delta\sigma_l\sigma_j\rangle_{ind}\langle\Delta\sigma_i\rangle_{ind}=0.$$

Similarly for other terms in $\xi^p(V)$, a direct calculation yields $\langle \xi^p(V)\sigma_j\rangle_{ind}=0$. From Equation (6.21), we have

$$\bar{\sigma}_j=\langle\sigma_j\rangle_n=\langle\sigma_j\rangle_{ind},$$

which can also be seen as follows: $P_{obs}(V)$ is a perturbation of $P_{ind}(V)$ in Equation (6.19); The perturbation $\xi^p(V)$ has mean zero with respect to $P_{ind}(V)$ because

$$\begin{aligned}\sum_V \xi^p(V)P_{ind}(V)&=\sum_V[1+\xi^p(V)]P_{ind}(V)-1\\&=\sum_V P_{obs}(V)-1\\&=0.\end{aligned}$$

Therefore, the mean value of σ_j is the same with respect to $P_{ind}(V)$ or $P_{obs}(V)$.

From Equation (6.20), we can obtain

$$\bar{\sigma}_j=\langle\sigma_j\rangle_n=\langle\sigma_j\rangle_{ind}=(1+\exp(-J_j^p))^{-1}. \tag{6.23}$$

For $i\neq j$, the correlation between the ith and the jth neurons is defined as

$$C_{ij}\equiv\langle\Delta\sigma_i\Delta\sigma_j\rangle_n,$$

then,

$$\begin{aligned}C_{ij}&=\sum_V(1+\xi^p(V))P_{ind}(V)\Delta\sigma_i\Delta\sigma_j\\&=\langle\Delta\sigma_i\Delta\sigma_j\rangle_{ind}+\langle\xi^p(V)\Delta\sigma_i\Delta\sigma_j\rangle_{ind}.\end{aligned}$$

Since σ_i and σ_j for $i\neq j$ are independent under P_{ind}, we have $\langle\Delta\sigma_i\Delta\sigma_j\rangle_{ind}=0$. From the expression of ξ^p and the above procedure of computing $\langle\xi^p(V)\sigma_j\rangle_{ind}$, we have

$$\langle\xi^p(V)\Delta\sigma_i\Delta\sigma_j\rangle_{ind}=\left\langle J_{ij}^p(\Delta\sigma_i)^2(\Delta\sigma_j)^2\right\rangle_{ind}.$$

Since $\left\langle(\Delta\sigma_i)^2\right\rangle_{ind}=\bar{\sigma}_i(1-\bar{\sigma}_i)$, we arrive at

$$C_{ij}=\bar{\sigma}_i(1-\bar{\sigma}_i)\bar{\sigma}_j(1-\bar{\sigma}_j)J_{ij}^p. \tag{6.24}$$

For $i\neq j$, $j\neq k$, $i\neq k$, the correlation among neurons i, j, k is defined as

$$C_{ijk}\equiv\langle\Delta\sigma_i\Delta\sigma_j\Delta\sigma_k\rangle_n.$$

Similarly, we have

$$C_{ijk}=\bar{\sigma}_i(1-\bar{\sigma}_i)\bar{\sigma}_j(1-\bar{\sigma}_j)\bar{\sigma}_k(1-\bar{\sigma}_k)J_{ijk}^p. \tag{6.25}$$

As we can see from Equations (6.24) and (6.25), the correlations are determined by the same order interactions of the distribution. Following [29], to construct a distribution $q(V)$ with the same form in Equation (3.1) whose correlations match those of $P_{obs}(V)$ up to a certain order, one simply needs to ensure that the parameters of the constructed distribution, J_i, J_{ij}, J_{ijk}, etc., are identical to those of the observed distributions, as seen in Equations (6.24) and (6.25). Since $q(V)$ is an approximation of $P_{obs}(V)$, we therefore can also assume that the strengths of high order interactions

of $q(V)$ are much smaller than the first order interaction. In particular, for any distribution $q(V)$, whose first order correlation matches that of the distribution $P_{obs}(V)$ and has the MaxEnt form as in Equation (3.1), following the procedure in [29], we have

$$q(V) = P_{ind}(V)(1+\xi^q(V)),$$

where $P_{ind}(V)$ is defined in Equation (6.20) and

$$\xi^q \equiv \sum_{i<j} J^q_{ij}\Delta\sigma_i\Delta\sigma_j + \sum_{i<j<k} J^q_{ijk}\Delta\sigma_i\Delta\sigma_j\Delta\sigma_k + h.o.t..$$

If we want to use the first order MaxEnt model to fit the distribution $P_{obs}(V)$, we only need to match the first order correlation (mean value) and simply let $\xi^q = 0$. Similarly, if we want to use the second order MaxEnt model to fit the distribution $P_{obs}(V)$ with identical second order correlations, we can set $J^q_{ij} = J^p_{ij}$ and other high order interactions to zero. The KL divergence of $P_{obs}(V)$ with respect to $q(V)$ can be written as

$$D_{KL}(P_{obs}||q) = \langle T(\xi^p(V), \xi^q(V))\rangle_n, \tag{6.26}$$

where

$$T(x,y) = \log(1+x) - \log(1+y).$$

If $x = y+\beta$ and β is a small number, Taylor expansion yields

$$T(x,y) = \frac{\beta}{1+y} + o(\beta).$$

By letting $x = \xi^p(V)$, $y = \xi^q(V)$, if $q(V)$ is the first order MaxEnt model, which will be denoted as $q_1(V)$, then

$$\beta = \sum_{i<j}^{n} J^p_{ij}\Delta\sigma_i\Delta\sigma_j + \sum_{i<j<k}^{n} J^p_{ijk}\Delta\sigma_i\Delta\sigma_j\Delta\sigma_k + h.o.t.,$$

and $\xi^q(V)$ equals 0 as discussed above. Therefore,

$$D_{KL}(P_{obs}||q_1) = \langle\beta\rangle_n. \tag{6.27}$$

For the sake of illustration, we consider n neurons within an all-to-all connected homogeneous network and assume that the linearity condition (6.9) holds. The conditional probability p is defined as follows

$$p = P(\sigma_1 = 1 | \sigma_i = 0 \text{ for } 2 \le i \le n), \tag{6.28}$$

through the nth order MaxEnt model (3.1), we have

$$p = (1+\exp(-J_1))^{-1}. \tag{6.29}$$

Since J^p_1 in Equation (6.23) is from the observed distribution $P_{obs}(V)$ which is the same as the distribution obtained by the nth order MaxEnt model, then $J^p_1 = J_1$. By Equations (6.23) and (6.29), we have

$$p = \bar{\sigma}_1.$$

By homogeneity, *i.e.*, $\delta_i = \delta$ and $p = \bar{\sigma}_i$ for $i = 1, 2, \cdots n$, where δ is the probability increment caused by one of the other neurons, from Equation (6.24), we can obtain

$$\begin{aligned}\langle \sum_{i<j} J_{ij}^p \Delta\sigma_i \Delta\sigma_j \rangle_n &= C_n^2 J_{12}^p \langle \Delta\sigma_i \Delta\sigma_j \rangle_n \\ &= C_n^2 (J_{12}^p)^2 p^2 (1-p)^2 \qquad (6.30) \\ &= C_n^2 \delta^2, \qquad (6.31)\end{aligned}$$

in which the last equality is obtained by substituting J_{12} in Equation (6.6) into Equation (6.30). Similarly, we have

$$\langle \sum_{i<j<k} J_{ijk}^p \Delta\sigma_i \Delta\sigma_j \Delta\sigma_k \rangle_n = C_n^3 \frac{(2p-1)^2}{p(1-p)} \delta^4. \qquad (6.32)$$

Substituting Equation (6.31) into Equation (6.27), to order $\mathcal{O}(\delta^2)$, we obtain

$$D_{KL}(P_{obs} || q_1) = C_n^2 \delta^2 + \mathcal{O}(\delta^4), \qquad (6.33)$$

If $q_2(V)$ is the second order MaxEnt model, then

$$\beta = \sum_{i<j<k}^{n} J_{ijk}^p \Delta\sigma_i \Delta\sigma_j \Delta\sigma_k + h.o.t.,$$

$$\xi^q(V) = \sum_{i<j} J_{ij}^p \Delta\sigma_i \Delta\sigma_j,$$

then, to order $\mathcal{O}(\delta^4)$,

$$D_{KL}(P_{obs} || q_2) = C_n^3 \frac{(2p-1)^2}{p(1-p)} \delta^4 + \mathcal{O}(\delta^6). \qquad (6.34)$$

Therefore, by substituting Equations (6.33) and (6.34) into the definition of f_I in Equation (6.18), we arrive at

$$f_I = 1 - \frac{C_n^3}{C_n^2} \frac{(2p-1)^2}{p(1-p)} \delta^2 + \mathcal{O}(\delta^4). \qquad (6.35)$$

For the nonhomogeneous case, if $\delta_{max} \ll p$, where $\delta_{max} = \max_i \delta_i$, since the interaction strengths also form a hierarchy in the power of δ_{max}, we still have $1 - f_I \sim \mathcal{O}(\delta_{max}^2)$. □

REMARK 6.2. Note that there is one-to-one correspondence between the correlations and the interactions, *e.g.*, in Equations (6.24) and (6.25). Therefore, the correlations also form a hierarchy in the power of δ, that is, the second order correlations have the dominate order δ while the third order correlations are of order δ^2 and so forth.

We use a network of three excitatory HH neurons with all-to-all connections to show the validity of Equation (6.35). The coupling strength is $s = 0.014\,\mathrm{ms}^{-1}$ (The corresponding physiological excitatory postsynaptic potential is $\sim 0.2\,\mathrm{mV}$). The input parameters are chosen as $\mu = 0.9\,\mathrm{ms}^{-1}$ (Poisson input rate) and $f = 0.056\,\mathrm{ms}^{-1}$ (Poisson input magnitude). The mean interspike interval is 27ms. We recorded the neuronal activity for a long time of 5.4×10^6 s in the simulation. All three neurons are selected to

carry out the MaxEnt model analysis with a sampling time bin size of 10ms. Through the fitting process, *i.e.*, the interaction strengths of the first and the second order MaxEnt model are estimated by an iterative method (See Appendix for details.), the value of $1-f_I$ in Equation (6.18) is 2.9×10^{-5}. We can also derive p in Equation (6.28) and δ (Here we use the mean value of δ_2 and δ_3 for δ.) from the observed distribution, then the approximate value of $1-f_I$ is 2.7×10^{-5}. These two results are rather close.

As we have mentioned above, the probability increment δ is rather small in an asynchronously firing network. Under the linearity condition, a sufficiently small δ leads to two facts: One is that high order interactions are weak compared to the low order ones as shown in Equation (6.11); The other is that, as shown in Equation (6.35), the multi-information fraction f_I is very close to 1. As demonstrated above, $f_I \geq 99\%$ for our model networks. It ranges from 90% to 99% in reported experiments [34,36,41]. The multi-information fraction f_I near unity signifies that the second order MaxEnt model can well capture the observed distribution of neuronal spiking patterns. Therefore, it is crucial to verify the linearity condition in neuronal networks. This will be discussed in detail in the following section.

7. Numerical verification

In the perturbative analysis discussed above, we can conclude that, under the linearity condition, the interaction strengths of the MaxEnt model form a hierarchy in the power of the probability increment δ. We now verify numerically that this linearity condition holds well in most dynamical regimes of neuronal networks as long as the network is asynchronous. We will use the spike trains generated from a full simulation of HH neuronal networks to carry out this verification.

First, we select a neuron, labeled as Neuron 1, to examine the linearity index R_T defined in Equation (6.9) for the numerical results of the neuronal network as shown in Figure 5.1. For a given sampling time bin size and a given subset size $N(T)=2,3$, we select all subsets T, with size $N(T)$, of all neurons excluding Neuron 1. Then, we compute the mean and standard deviation of all R_T over the selected subsets. The results are shown in Figure 5.1C, in which the dashed and solid black lines stand for the case of $N(T)=2$ and $N(T)=3$, respectively. It can be seen clearly that the linearity index R_T in this network is nearly unity. As is shown in our perturbative analysis of the MaxEnt model, P_2 can then provide a good approximation to the spiking pattern distribution for the group of selected neurons. It is worthwhile to point out that the third, fourth, and fifth order interactions are of the same order as seen in Figure 5.1A. The reason why there is no order of magnitude difference among these higher order interactions is as follows: Under the strict linearity condition, the kth order interaction has the leading order term of $\mathcal{O}(\delta^{k-1})$; However, the linearity condition in general does not hold exactly. As is shown in Equation (6.7), there are terms of δ order less than $k-1$ appearing in the kth order interaction. To see this effect in a concrete example, we assume the linearity condition does not hold strictly in a homogeneous network and pick probability increments, say, as follows:

$$P(\sigma_1=1|\sigma_2=1,\sigma_3=1,\sigma_4=0)=p+1.97\delta, \tag{7.1}$$

$$P(\sigma_1=1|\sigma_2=1,\sigma_3=1,\sigma_4=1)=p+3.05\delta. \tag{7.2}$$

Note that the numerical values of 1.97 and 3.05 in the coefficient of δ are chosen arbitrarily, for which the linearity condition does not hold exactly. We further choose $p=0.2$, $\delta=0.03$, then, the interaction strengths can be estimated to be $J_1=-1.3863$,

$J_{12}=0.1770,\ J_{123}=-0.0255,\ J_{1234}=0.0193$ through the analytic solution of interactions, such as Equation (4.14). In this numerical example, J_{123} and J_{1234} are of the same order, whereas both are one order of magnitude smaller than J_{12}. Incidentally, we compute a fundamental term in Equation (4.14) as an illustration. By homogeneity, neurons are equivalent, then we have $\log P(\sigma_1=1|\sigma_2=0,\sigma_3=1,\sigma_4=1)=p+1.97\delta$ as Equation (7.1). As mentioned above, we can write a fundamental term in terms of conditional probabilities

$$\log\frac{P_{1011}}{P_{0011}}=\log\frac{P(\sigma_1=1|\sigma_2=0,\sigma_3=1,\sigma_4=1)}{P(\sigma_1=0|\sigma_2=0,\sigma_3=1,\sigma_4=1)}$$
$$=\log\frac{p+1.97\delta}{1-(p+1.97\delta)}.$$

We further examine whether the linearity condition and reconstruction of the distribution of neuronal firing patterns are dependent of a particular dynamical regime. Dynamical regimes are often realized by a particular choice of network system parameters. We investigate this issue by scanning the magnitude f and the rate μ in the Poisson drive of HH neuronal networks. The scanned range of these parameters produces network dynamics with the range of firing rates ($3\text{Hz}-50\text{Hz}$) of real neurons. Note that there are typically three dynamical regimes for the HH neuronal network with fixed input magnitude f [49, 50]: (i) a highly fluctuating regime when the input rate μ is low; (ii) an intermediate regime when μ is moderately high; (iii) a low fluctuating or mean driven regime when μ is very high. The HH network which we use consists of 80 excitatory and 20 inhibitory neurons. We select 10 neurons at random from the network to perform the MaxEnt model analysis. The sampling time bin size is selected as in common experimental settings, such as 10ms [14, 21, 26, 27, 36, 48]. Since the time duration of spike width and refractory period are on the order of 3ms, 10ms is sufficiently short to avoid more than one spike in a bin. As is shown in the first and the second rows in Figure 7.1, we select two kinds of network coupling to perform the MaxEnt model analysis. In addition to the coupling topology described by random connections, we also choose a band adjacency matrix to further investigate whether our analysis can provide insights into networks dynamics with other topologies. The underlying coupling structure for the first row (A-C) of Figure 7.1 is described by a band adjacency matrix, *i.e.*, each neuron is connected to its neighboring 20 postsynaptic neurons. For the second row (D-F) of Figure 7.1, it is a network of homogeneous random connections with connection probability 0.2. For both coupling structures, the coupling strength between two connected neurons is selected at random based on the uniform distribution between 0 and 1mV. We examine the linearity index R_T in Equation (6.9) on the subsets excluding neuron 1 with size $N(T)=2$. For a given parameter pair of μ (ordinate) and $f\mu$ (abscissa) at the lower left corner of each box in Figure 7.1A and D, most mean values of R_T are very close to unity. For both network structures, an example of reconstructed distribution for the input of $\mu=0.9\text{ms}^{-1}$ and $f=0.033\text{ms}^{-1}$ (green box in Figure 7.1A and D) is shown in Figure 7.1B and E, respectively, the reconstructed distribution of the second order MaxEnt model P_2 is in good agreement with the direct measurement of the distribution from the numerical simulation.

For a dynamical state to be linear in the sense of $R_T\approx 1$, the firing dynamics of the network cannot be too synchronized. As exemplified in one of cases in Figure 7.1A and D, for which $\mu=0.9\text{ms}^{-1}$ and $f=0.033\text{ms}^{-1}$ (green box in Figure 7.1A and D), the corresponding raster plot is shown in Figure 7.1C and F, in which neurons are in an

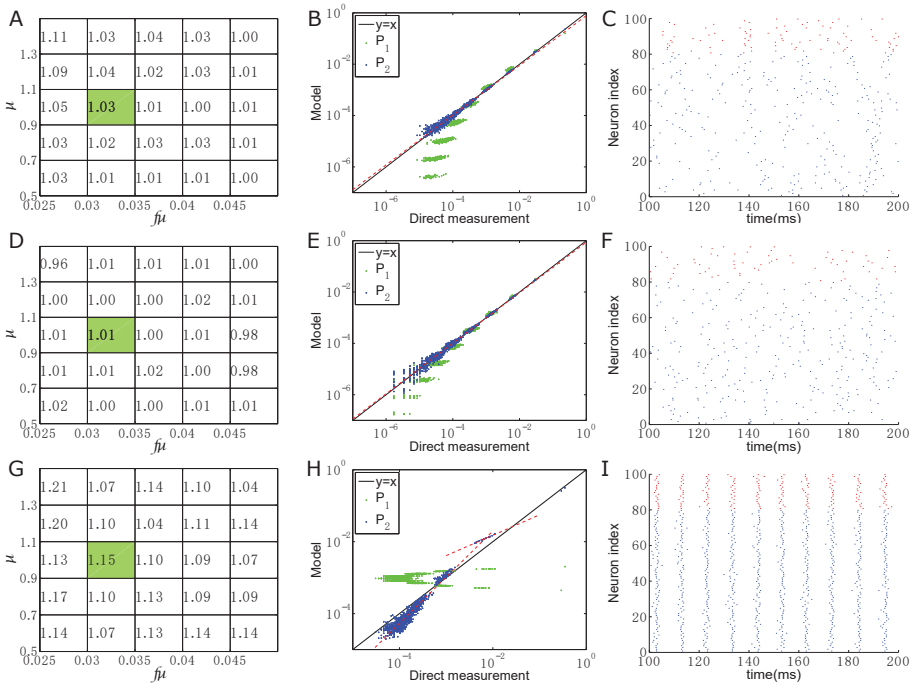

FIG. 7.1. **Linearity index and MaxEnt model peformance in different dynamical regimes of HH neuronal networks.** *The network consists of* 100 *HH neurons (*80 *Excitatory and* 20 *Inhibitory) driven by Poisson inputs. The underlying coupling structure for the first row (A-C) is described by a band adjacency matrix,* i.e., *each neuron is connected to its neighboring* 20 *postsynaptic neurons. For the second and the third rows (D-I), these are networks with random connections with connection probability* 0.2. *The coupling strength is selected at random from the uniform distribution of the interval* $[0,s]$, *where* $s=0.0714\text{ms}^{-1}$ *for (A-F) and* $s=0.429\text{ms}^{-1}$ *for (G-I) (The corresponding physiological excitatory/inhibitory postsynaptic potential is* $\sim 1\text{mV}$ *and* $\sim 6\text{mV}$ *for* $s=0.0714\text{ms}^{-1}$ *and* 0.429ms^{-1}, *respectively.). The scanning parameters produce a network with firing rates* $3\text{Hz}-50\text{Hz}$ *for (A-F) and* $30\text{Hz}-50\text{Hz}$ *for (G-I).* 10 *neurons are selected at random to perform the MaxEnt model analysis. The sampling time bin size is selected to be* 10ms. *The total recording time is* $2\times 10^4\text{s}$. *(A, D, G) The number in each box is the mean value of the linearity index* R_T *[Equation (6.9)] of all subsets excluding neuron 1 with size* $N(T)=2$ *for a given parameter pair of* μ *(ordinate) and* $f\mu$ *(abscissa) at the lower left corner of each box. For A and D, the standard deviation of* R_T *for each input is less than* 0.03, *except for the input of* $f\mu=0.025$ *and* $f\mu=0.03$ *with* $\mu=1.3$ *(The left two boxes of the first row in A and D), where their standard deviations of* R_T *are less than* 0.08 *and their corresponding firing rates are less than* 5Hz. *(B, E, H) For the inputs of the green boxes in the left column (A, D, G), the corresponding rate of occurrence of each firing state predicted from the MaxEnt model distribution of the second order* P_2 *(blue) and the distribution of the first order MaxEnt model* P_1 *(green) is plotted against the measured occurrence rate generated from the numerical simulation. We perform the linear fitting in the log-log plot for data points in (B), (E) and (H). The slopes of the linear fitting (dashed red line) are* 0.97 *and* 0.98 *for (B) and (E), respectively. Since the points of* P_2 *in (H) have two distinct regions with different slopes, we perform a linear fitting in the log-log plot in both regions. The slope of the linear fitting (dashed red lines) is* 0.56 *and* 1.28 *for the upper and lower regions, respectively. (C, F, I) For the inputs of the green boxes in left column (A, D, G), the corresponding raster plot for inhibitory and excitatory neurons in the network is shown by the red and blue dots, respectively.*

asynchronously firing state. We also show a numerical case in the third row in Figure 7.1 with Poisson inputs, for which the dynamics of the network is rather synchronized. The network in the third row (G-I) of Figure 7.1 has random connections with connection

probability 0.2, and the coupling strength is uniformly selected at random between 0 and 6 mV—a stronger coupling strength than the first two rows in Figure 7.1. To see how well neurons are synchronized, we show a raster plot of this synchronous network in Figure 7.1I, for which $\mu = 0.9\,\mathrm{ms}^{-1}$ and $f = 0.033\,\mathrm{ms}^{-1}$ (green box in Figure 7.1G). To characterize the degree of synchronization of the dynamics, as discussed in Section 3, we use the KL divergence D_1 as a synchronization index. The synchronization indexes for the state in Figure 7.1A and D are smaller than 0.2 whereas all the synchronization indexes of the selected 10 neurons in Figure 7.1G are more than 3.1. For this synchronous subnetwork, most of the mean values of R_T of all subsets excluding neuron 1 with size $N(T) = 2$ exhibit a significant deviation from unity. For example, the mean value of R_T of the green box in Figure 7.1G is 1.15 ± 0.04 (mean ± SEM (Standard Error of the Mean)). Meanwhile, as is shown in Figure 7.1H, the reconstructed distribution of the second order MaxEnt model is not consistent with the direct measurement of the distribution from the numerical simulation. The data points exhibit a clear deviation from the line $y = x$ in Figure 7.1H. Since the points of P_2 in Figure 7.1H have two distinct regions with different slopes, we perform a linear fitting in the log-log plot for each region. The slope of the linear fitting for the upper (lower) region in Figure 7.1H is 0.56 (1.28) while the slopes of the linear fitting are 0.97 and 0.98 for Figure 7.1B and E, respectively. These slopes give a simple assessment of how well P_2 approximates the observed distribution. Clearly, P_2 fails to capture the observed distribution in synchronous networks, in which the linearity condition is no longer valid.

8. Discussions

As described above, in a neuronal network whose dynamics is not too synchronized, the linearity condition holds rather well, therefore, the strengths of high order interactions are much smaller than the low orders. However, the fact that the linearity condition does not hold exactly in the neuronal data leads to a result that the strengths of high order interactions (above the third order) in the nth order MaxEnt model are comparable to those of the third order. In addition, for a group of n neurons selected for a MaxEnt model analysis, the number of interactions of all orders is $2^n - 1$ whereas the number of the first order and the second order interactions in total is $n(n+1)/2$. As the group size grows, *i.e.*, n increases, the percentage of interactions of low orders $[n(n+1)/2]/(2^n - 1)$ decreases exponentially. Therefore, even in an asynchronous neuronal network, as the selected neuronal group size increases, the percentage of high order interactions whose strengths are comparable to those of the third order becomes large. Therefore, the effect of high order interactions may become important. This could be the reason underlying the phenomenon observed in experiments that the second order MaxEnt model is no longer sufficient for a large group of selected neurons [12].

Using our theoretical framework, we investigate some other important issues related to the MaxEnt model: (i) How the sampling time bin size affects the results above? (ii) Why the success of the MaxEnt model is not simply a consequence of weak correlations?

8.1. Bin size. Experimental works have shown that the second order MaxEnt model performs better for the case of larger bin sizes ($\sim 20\,\mathrm{ms}$) than smaller bin sizes ($\leq 4\,\mathrm{ms}$) [36, 41]. It is natural to ask the question of how the bin size affects our above results. For a homogeneous network with all-to-all connections, under the linearity condition, the leading order term of the ratio J_{123}/J_{12} is

$$\frac{J_{123}}{J_{12}} \approx \frac{(2p-1)}{p(1-p)}\delta. \tag{8.1}$$

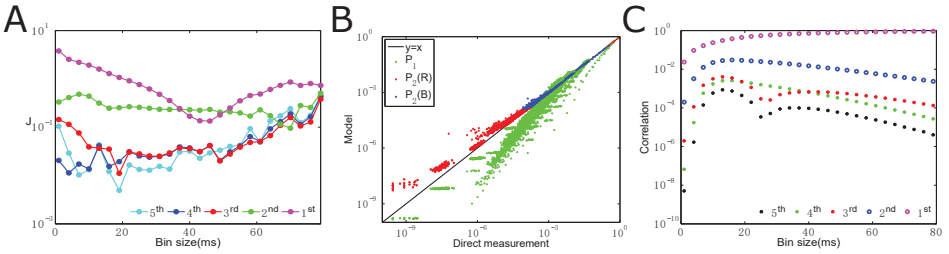

FIG. 8.1. *Sensitivity to bin size and dependence on correlations. The simulation is for a network of eight excitatory HH neurons with all-to-all connections. The coupling strength is* $s = 0.143\text{ms}^{-1}$ *(The corresponding physiological excitatory postsynaptic potential is* $\sim 2\text{mV}$*). The input parameters are chosen as* $\mu = 1\text{ms}^{-1}$ *and* $f = 0.035\text{ms}^{-1}$*. The mean interspike interval is* 42ms*. The total recording time is* 1.2×10^7s*. All* 8 *neurons are selected to carry out the MaxEnt model analysis. (A) Colored lines correspond to different orders of interactions. The data point is the mean absolute value of interaction strengths of the corresponding order for different sampling time bin sizes, the first order (magenta), the second order (green), the third order (red), the fourth order (blue), and the fifth order (cyan). (B) The rate of occurrence of each firing state predicted from the distribution of the second order MaxEnt model* P_2 *(The red points are for bin size of* $1\text{ms} - 4\text{ms}$ *and* $55\text{ms} - 79\text{ms}$ *whereas the blue points are for bin size of* $7\text{ms} - 52\text{ms}$*.) and the distribution of the first order MaxEnt model* P_1 *(green) is plotted against the measured occurrence rate generated from the numerical simulation. (C) Dots and circles correspond to different orders of correlations. The data point is the mean absolute value of correlation strengths of the corresponding order for different sampling time bin sizes, mean (magenta), the second order (blue), the third order (red), the fourth order (green), and the fifth order (black).*

When p is close to 1 or 0, the denominator of Equation (8.1) becomes very small and J_{123} is no longer much smaller than J_{12}. Statistically, it is easier to find a neuron firing in a larger bin size than in a smaller bin size. Hence, the conditional probability p increases as the sampling time bin size increases. J_{123} is no longer smaller than J_{12} for a sampling time bin of very small or very large size. Figure 8.1 displays a sensitivity analysis result for a homogeneously coupled HH neuronal network of 8 neurons driven by Poisson inputs. The mean interspike interval of each neuron is 42ms. We record the spike trains of all eight neurons for 1.2×10^7s, which is sufficiently long to reliably obtain a stable distribution of neuronal firing patterns. We perform the MaxEnt model analysis for all eight neurons using different bin sizes, ranging from 1ms to 79ms. As is shown in Figure 8.1A, a sampling time bin of very small ($1\text{ms} - 4\text{ms}$) or very large size ($67\text{ms} - 79\text{ms}$) would render the mean strengths of high order interactions no longer much smaller (in the absolute value) than the lower order ones. For the small bin size of $1\text{ms} - 4\text{ms}$ and large bin size of $55\text{ms} - 79\text{ms}$, as is shown by the red dots in Figure 8.1B, some firing events occur very rarely. Without high order interactions, the probabilities of these rare events cannot be well approximated by the second order MaxEnt model. When the bin size is in $7\text{ms} - 52\text{ms}$, the mean strengths of high order interactions are nearly one order of magnitude smaller than those of the first two orders (as shown in Figure 8.1A), the reconstructed distribution of the second order MaxEnt model is in good agreement with observed distributions (blue dots in Figure 8.1B). From Figure 8.1A, we can see that a sampling time bin of very small or very large size would lead to rather large strengths of high order interactions, thus giving rise to the failure of the second order MaxEnt model.

8.2. Correlation. As often observed, the correlation coefficient between the activity of two neurons is typically weak ($\leq 10\%$) [1, 7], one may suspect that the weak correlations might underpin the success of the second order MaxEnt model. However, as

discussed in Section 1, there are theoretical analyses [1] using a perturbation theory to show that the success of the second order MaxEnt model is not directly related to weak correlations. Instead of focusing on weak correlations, we perform the perturbation theory with respect to the probability increment δ. Our analysis can be applied to understand more specifically why the success of the second order MaxEnt model is not simply a consequence of weak correlations. We examine an example of n neurons with homogeneous connections under the linearity condition. For correlations, from Equations (6.24) and (6.25), we can obtain the leading order term of the ratio C_{123}/C_{12} as follows

$$\frac{C_{123}}{C_{12}} \approx (2p-1)\delta. \tag{8.2}$$

For p close to 1 or 0 , from Equations (8.1) and (8.2), we can see that the high order interaction J_{123} can be much larger than the low order interaction J_{12}, meanwhile, the high order correlation C_{123} is much smaller than C_{12}. This situation can also be observed in our numerical simulations. In Figure 8.1C, at the sampling time bin size of 79 ms, the high order correlations are at least one order of magnitude smaller than those of the first two orders. However, the strengths of high order interactions are comparable to those of the low order ones (as shown in Figure 8.1A). Therefore, the success of a second order MaxEnt model is not simply a consequence of weak correlations of higher orders.

9. Conclusion

To understand the validity of the second order MaxEnt model for neuronal networks, we have explored network dynamical states in which the linearity condition persists. We have developed a perturbative analysis to show that, under such dynamical state, the strengths of high order interactions are much smaller than those of the lower order ones, thus, giving rise to the fact that a second order MaxEnt model can capture well the observed distribution of neuronal firing patterns. We have verified that the linearity condition holds rather well in asynchronous neuronal networks. Based on our theoretical framework, we have rationalized why the second order MaxEnt model is not sufficient for a recorded neuron group of large size as a consequence of the cumulative effect of high order interactions of the nth order MaxEnt model. We have also discussed that a sampling time bin of very small or very large size would lead to rather large strengths of high order interactions, thus, giving rise to the failure of the second order MaxEnt model. We have further shown that even when high order correlations are weak, high order interactions in the MaxEnt model can still be very large. This leads to the conclusion that the success of the second order MaxEnt model is not simply a consequence of weak correlations.

Acknowledgments. This work was supported by Grant No. NSFC-91230202, NSFC-11671259 and Shanghai Rising-Star Program-15QA1402600 (D.Z.); by NSF DMS-1009575 and NSFC-31571071 (D.C.); by Shanghai 14JC1403800, 15JC1400104, and SJTU-UM Collaborative Research Program (D.C. and D.Z.); and by the NYU Abu Dhabi Institute G1301 (Z.X., D.Z., and D.C.).

Appendix A.

A.1. Iterative methods for obtaining interaction strengths in MaxEnt models. Numerically, we use the same iteration method as in [41] to estimate the parameters of the MaxEnt model in Equation (3.1) for m less than n. For completeness, we use the second order MaxEnt model as an example to briefly illustrate the iteration

method. At the first level of approximation, the values of the interactions are given as follows: $J_i = \langle \sigma_i \rangle_E$ and $J_{ij} = \langle \sigma_i \sigma_j \rangle_E$. This initializes the distribution $P_2(V)$ of the second order MaxEnt model. The expected values of the individual mean values $\langle \sigma_i \rangle_2$ and pairwise correlations $\langle \sigma_i \sigma_j \rangle_2$ with respect to the distribution $P_2(V)$ can now be determined by

$$\langle \sigma_i \rangle_2 \equiv \sum_V \sigma_i(V) P_2(V),$$

$$\langle \sigma_i \sigma_j \rangle_2 \equiv \sum_V \sigma_i(V) \sigma_j(V) P_2(V),$$

where $\sigma_i(V)$ is the activity of the ith neuron in the state V. To improve the agreement between $\langle \sigma_i \rangle_2$, $\langle \sigma_i \sigma_j \rangle_2$ and $\langle \sigma_i \rangle_E$, $\langle \sigma_i \sigma_j \rangle_E$, the values of J_i and J_{ij} are adjusted by an iterative procedure:

$$J_i^{new} = J_i^{old} + \alpha \text{sign}\left(\langle \sigma_i \rangle_E\right) \log \frac{\langle \sigma_i \rangle_E}{\langle \sigma_i \rangle_2},$$

$$J_{ij}^{new} = J_{ij}^{old} + \alpha \text{sign}\left(\langle \sigma_i \sigma_j \rangle_E\right) \log \frac{\langle \sigma_i \sigma_j \rangle_E}{\langle \sigma_i \sigma_j \rangle_2},$$

in which the constant α is used to maintain the stability of the iteration, $\text{sign}(x)$ is the sign of the number x. We use $\alpha = 0.75$ as in [41]. Adjustments are performed for 5×10^4 iterations for each ensemble until the J_i and J_{ij} were within 0.1% of tolerance. It usually takes less than 5×10^4 iterations to reach this desired accuracy for each ensemble. We note that the above iterative method can be easily extended to estimate higher orders of interactions in the MaxEnt model.

REFERENCES

[1] F. Azhar and W. Bialek, *When are correlations strong?*, preprint, arXiv:1012.5987, 2010.

[2] A.K. Barreiro, J. Gjorgjieva, F. Rieke, and E. Shea-Brown, *When do microcircuits produce beyond-pairwise correlations?*, Front. Comput. Neurosc., 8:10, 2014.

[3] J. Barton and S. Cocco, *Ising models for neural activity inferred via selective cluster expansion: structural and coding properties*, J. Stat. Mech. Theor. Exp., P03002, 2013.

[4] A. Borst and F.E. Theunissen, *Information theory and neural coding*, Nat. Neurosci., 2:947–957, 1999.

[5] T. Broderick, M. Dudik, G. Tkacik, R.E. Schapire, and W. Bialek, *Faster solutions of the inverse pairwise ising problem*, preprint, arXiv:0712.2437, 2007.

[6] A. Cavagna, I. Giardina, F. Ginelli, T. Mora, D. Piovani, R. Tavarone, and A.M. Walczak, *Dynamical maximum entropy approach to flocking*, Phys. Rev. E , 89:042707, 2014.

[7] M.R. Cohen and A. Kohn, *Measuring and interpreting neuronal correlations*, Nat. Neurosci., 14:811–819, 2011.

[8] Y. Dan, J.-M. Alonso, W.M. Usrey, and R.C. Reid, *Coding of visual information by precisely correlated spikes in the lateral geniculate nucleus*, Nat. Neurosci., 1:501–507, 1998.

[9] B. Dunn, M. Mørreaunet, and Y. Roudi, *Correlations and functional connections in a population of grid cells*, PLoS Comput. Biol., 11:e1004052, 2011.

[10] E. Ferrea, A. Maccione, L. Medrihan, T. Nieus, D. Ghezzi, P. Baldelli, F. Benfenati, and L. Berdondini, *Large-scale, high-resolution electrophysiological imaging of field potentials in brain slices with microelectronic multielectrode arrays*, Front. Neural Circuits, 6:80, 2012.

[11] E. Ganmor, R. Segev, and E. Schneidman, *The architecture of functional interaction networks in the retina*, J. Neurosci., 31:3044–3054, 2011.

[12] E. Ganmor, R. Segev, and E. Schneidman, *Sparse low-order interaction network underlies a highly correlated and learnable neural population code*, Proc. Natl. Acad. Sci. U.S.A., 108:9679–9684, 2011.

[13] A. Golan, G.G. Judge, and D. Miller, *Maximum Entropy Econometrics: Robust Estimation with Limited Data*, Wiley, New York, 1996.
[14] E. Granot-Atedgi, G. Tkačik, R. Segev, and E. Schneidman, *Stimulus-dependent maximum entropy models of neural population codes*, PLoS Comput. Biol., 9:e1002922, 2013.
[15] A. Hernando, R. Hernando, A. Plastino, and A. Plastino, *The workings of the maximum entropy principle in collective human behaviour*, J. R. Soc. Interface, 10:20120758, 2013.
[16] J. Hertz, Y. Roudi, and J. Tyrcha, *Ising models for inferring network structure from spike data*, in Principles of Neural Coding, CRC Press, 2013.
[17] E.T. Jaynes, *Information theory and statistical mechanics*, Phys. Rev., 106:620–630, 1957.
[18] S. Khatiwala, F. Primeau, and T. Hall, *Reconstruction of the history of anthropogenic co2 concentrations in the ocean*, Nature, 462:346–349, 2009.
[19] H. Lancaster, *The structure of bivariate distributions*, Ann. Math. Stat., 29:719–736, 1958.
[20] H. Lancaster, *Correlation and complete dependence of random variables*, Ann. Math. Stat., 34:1315–1321, 1963.
[21] J.H. Macke, M. Opper, and M. Bethge, *Common input explains higher-order correlations and entropy in a simple model of neural population activity*, Phys. Rev. Lett., 106:208102, 2011.
[22] A.B. Mantsyzov, A.S. Maltsev, J. Ying, Y. Shen, G. Hummer, and A. Bax, *A maximum entropy approach to the study of residue-specific backbone angle distributions in α-synuclein, an intrinsically disordered protein*, Protein Sci., 23:1275–1290, 2014.
[23] O. Marre, S. El Boustani, Y. Frégnac, and A. Destexhe, *Prediction of spatiotemporal patterns of neural activity from pairwise correlations*, Phys. Rev. Lett., 102:138101, 2009.
[24] F. Montani, R.A. Ince, R. Senatore, E. Arabzadeh, M.E. Diamond, and S. Panzeri, *The impact of high-order interactions on the rate of synchronous discharge and information transmission in somatosensory cortex*, Phil. Trans. R. Soc. A, 367:3297–3310, 2009.
[25] H. Nasser and B. Cessac, *Parameter estimation for spatio-temporal maximum entropy distributions: Application to neural spike trains*, Entropy, 16:2244–2277, 2014.
[26] H. Nasser, O. Marre, and B. Cessac, *Spatio-temporal spike train analysis for large scale networks using the maximum entropy principle and monte carlo method*, J. Stat. Mech. Theor. Exp., P03006, 2013.
[27] I.E. Ohiorhenuan, F. Mechler, K.P. Purpura, A.M. Schmid, Q. Hu, and J.D. Victor, *Sparse coding and high-order correlations in fine-scale cortical networks*, Nature, 466:617–621, 2010.
[28] I.E. Ohiorhenuan and J.D. Victor, *Information-geometric measure of 3-neuron firing patterns characterizes scale-dependence in cortical networks*, J. Comput. Neurosci., 30:125–141, 2011.
[29] Y. Roudi, S. Nirenberg, and P.E. Latham, *Pairwise maximum entropy models for studying large biological systems: when they can work and when they can't*, PLoS Comput. Biol., 5:e1000380, 2009.
[30] Y. Roudi, J. Tyrcha, and J. Hertz, *Ising model for neural data: model quality and approximate methods for extracting functional connectivity*, Phys. Rev. E, 79:051915, 2009.
[31] D. Sakakibara, A. Sasaki, T. Ikeya, J. Hamatsu, T. Hanashima, M. Mishima, M. Yoshimasu, N. Hayashi, T. Mikawa, M. Wälchli, et al., *Protein structure determination in living cells by in-cell nmr spectroscopy*, Nature, 458:102–105, 2009.
[32] S. Saremi and T.J. Sejnowski, *Hierarchical model of natural images and the origin of scale invariance*, Proc. Natl. Acad. Sci. U.S.A., 110:3071–3076, 2013.
[33] O. Sarmanov, *Maximum correlation coefficient (nonsymmetric case)*, Selected Transl. Math. Statist. and Probability, 2:207–210, 1962.
[34] E. Schneidman, M.J. Berry, R. Segev, and W. Bialek, *Weak pairwise correlations imply strongly correlated network states in a neural population*, Nature, 440:1007–1012, 2006.
[35] J. Shlens, G.D. Field, J.L. Gauthier, M. Greschner, A. Sher, A.M. Litke, and E. Chichilnisky, *The structure of large-scale synchronized firing in primate retina*, J. Neurosci., 29:5022–5031, 2009.
[36] J. Shlens, G.D. Field, J.L. Gauthier, M.I. Grivich, D. Petrusca, A. Sher, A.M. Litke, and E. Chichilnisky, *The structure of multi-neuron firing patterns in primate retina*, J. Neurosci., 26:8254–8266, 2006.
[37] J. Shlens, F. Rieke, and E. Chichilnisky, *Synchronized firing in the retina*, Curr. Opin. Neurobiol., 18:396–402, 2008.
[38] T. Squartini, I. van Lelyveld, and D. Garlaschelli, *Early-warning signals of topological collapse in interbank networks*, Sci. Rep., 3:3357, 2013.
[39] G.J. Stephens and W. Bialek, *Statistical mechanics of letters in words*, Phys. Rev. E, 81:066119, 2010.
[40] J.I. Sułkowska, F. Morcos, M. Weigt, T. Hwa, and J.N. Onuchic, *Genomics-aided structure prediction*, Proc. Natl. Acad. Sci. U.S.A., 109:10340–10345, 2012.
[41] A. Tang, D. Jackson, J. Hobbs, W. Chen, J.L. Smith, H. Patel, A. Prieto, D. Petrusca, M.I.

Grivich, A. Sher, et al., *A maximum entropy model applied to spatial and temporal correlations from cortical networks in vitro*, J. Neurosci., 28:505–518, 2008.
[42] G. Tkacik, *Information Flow in Biological Networks*, Princeton University, 2007.
[43] W. Truccolo, L.R. Hochberg, and J.P. Donoghue, *Collective dynamics in human and monkey sensorimotor cortex: predicting single neuron spikes*, Nat. Neurosci., 13:105–111, 2010.
[44] J.C. Vasquez, O. Marre, A.G. Palacios, M.J. Berry, and B. Cessac, *Gibbs distribution analysis of temporal correlations structure in retina ganglion cells*, J. Physiol. Paris, 106:120–127, 2012.
[45] T. Watanabe, S. Hirose, H. Wada, Y. Imai, T. Machida, I. Shirouzu, S. Konishi, Y. Miyashita, and N. Masuda, *A pairwise maximum entropy model accurately describes resting-state human brain networks*, Nat. Commun., 4:1370, 2013.
[46] F.-C. Yeh, A. Tang, J.P. Hobbs, P. Hottowy, W. Dabrowski, A. Sher, A. Litke, and J.M. Beggs, *Maximum entropy approaches to living neural networks*, Entropy, 12:89–106, 2010.
[47] S. Yu, D. Huang, W. Singer, and D. Nikolić, *A small world of neuronal synchrony*, Cereb. Cortex, 18:2891–2901, 2008.
[48] S. Yu, H. Yang, H. Nakahara, G.S. Santos, D. Nikolić, and D. Plenz, *Higher-order interactions characterized in cortical activity*, J. Neurosci., 31:17514–17526, 2011.
[49] D. Zhou, Y. Xiao, Y. Zhang, Z. Xu, and D. Cai, *Causal and structural connectivity of pulse-coupled nonlinear networks*, Phys. Rev. Lett., 111:054102, 2013.
[50] D. Zhou, Y. Xiao, Y. Zhang, Z. Xu, and D. Cai, *Granger causality network reconstruction of conductance-based integrate-and-fire neuronal systems*, PloS One, 9:e87636, 2014.